

# Mixing of an effusion film within a turbulent boundary layer

*Jeremy Basley\* and Kevin Gouder\*\* and Jonathan F. Morrison\*\**

\*LAMIH, CNRS UMR 8201, Université Polytechnique Hauts-de-France, INSA,  
Le Mont Houy, 59300 Valenciennes, France  
*jeremy.basley@uphf.fr*

\*\*Department of Aeronautics, Imperial College London, London SW7 2AZ, UK  
*kevin.gouder04@imperial.ac.uk and j.morrison@imperial.ac.uk*

## Abstract

The large-scale modulation of an effusion film injected into a high Reynolds-number boundary layer is investigated for a wide range of film-velocity to freestream-velocity ratios. Particle Image Velocimetry (PIV), visualisations and hot-wire measurements are used to characterise the momentum effects underlying the mixing of the effusion film. For this experiment, the geometry of a turbine blade is idealised in a largescale facility with a canonical upstream boundary layer where the effusion film and the boundary layer are isothermal. Spectral analysis shows that the injection of the effusion film first promotes near-wall turbulence until the film breaks away from the surface when the velocity ratio reaches a critical value. For higher velocity ratios, large-scale motions from the incoming boundary layer no longer penetrate the sublayer. The associated spectral signature is accompanied by enhanced inter-scale exchanges, as shown by the skewness of the streamwise velocity component and the amplitude modulation coefficients.

Use of seeding in the film flow enables the estimation of the concentration of injected fluid in the laser sheet. Joint momentum-concentration data show that the mixing of the film is strongly modulated by the large-scale motions of the turbulent boundary layer, although in different ways depending on the velocity ratio. For very low velocity ratios, largescale motions are largely unaffected by the film. They encompass the boundary layer down to the injected sublayer and modulate locally the concentration of injected film. For higher velocity ratios, mixing intensifies as the effusion film is injected with momentum and reaches further from the wall. As a result, the concentration of injected fluid in the near-wall region is remotely, yet more intensively modulated by the large-scale motions above the sublayer.

## 1. Introduction

In order to withstand the high temperature flows coming out of a combustion chamber, jet engine turbine blades require cooling by the use of low temperature bleed flows producing an effusion film. Typically, cooling flow rates are large: velocity ratios  $VR = U_f = U_\infty$  range from 1 to 3, where  $U_f$  and  $U_\infty$  are the characteristic velocities of the film and the incoming flow, respectively (for a review, see Krewinkel, 2013). For higher engine efficiency, a better understanding of the momentum and heat exchange between the effusion film and the boundary layer is required to deduce a minimal cooling flow rate while maintaining the integrity of the film. These highly distorted flows conform to the description of suddenly perturbed boundary layers. Generally, the turbulence does not adjust immediately to changes in the mean strain rate. In any case, these flows are far from equilibrium as the effects of the new surface condition are unlikely to have permeated the whole layer (for a review, see Smits & Wood, 1985). Detailed studies of perturbed boundary layers with changes to both momentum and heat flux are few: some exceptions are those by Subramanian & Antonia (1981); Andreopoulos (1983).

This experimental study focuses on low velocity ratios ( $VR < 0.4$ ) using an idealised, large geometry at low speed to enable spatial and temporal resolution that are much better than those available in typical turbine rigs. This allows us to highlight the momentum exchange mechanisms between the injected film and the incoming boundary layer at the cost of reduced relevance in neglecting such effects as blade rotation, freestream unsteadiness and turbulence, roughness and pressure gradients. A canonical turbulent boundary layer is injected with, in this case, an isothermal effusion film for a range of film velocity ratios (Figure 1, Bottom). The analysis focuses on the correlations between the concentration of injected fluid and the large-scale fluctuations of velocity. The solid surface condition is taken to be isothermal.

While the present measurements are isothermal, further simultaneous measurements of temperature and velocity (reported elsewhere) are made where the film emerges at a temperature of a few degrees below that of the boundary

layer so that the scalar field is passive, and results are directly comparable to those herein. It is well known that, even in unperturbed flows (close to a state of equilibrium), Reynolds analogy is a poor assumption (see, for example Kays & Moffat, 1988). For perturbed flows (such as boundary layers on turbine blades), the situation is even worse and large departures from Reynolds analogy are likely.

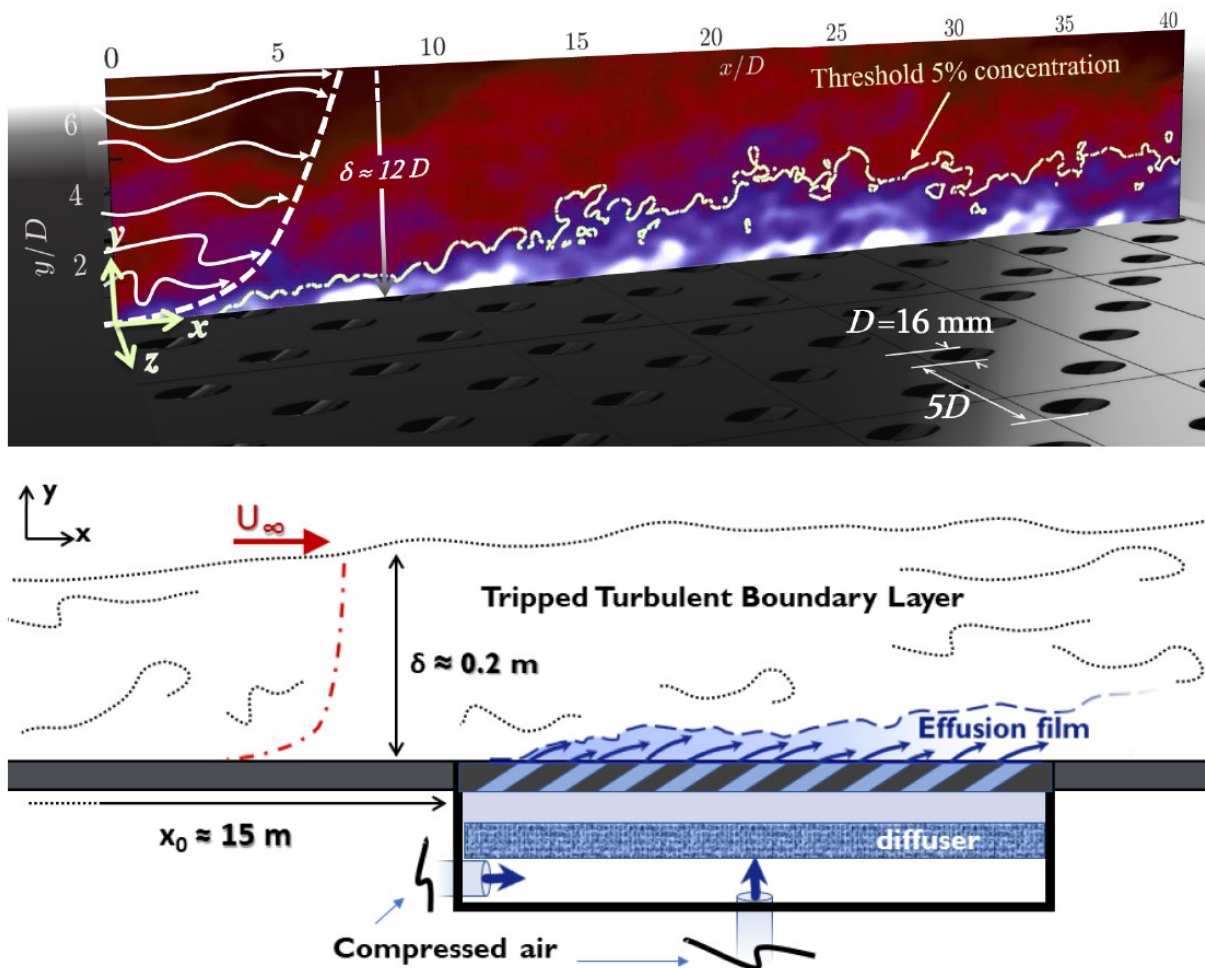


Figure 1: (Top) Rendered snapshot of streamwise velocity fluctuations superimposed with concentration of injected fluid (yellow line denotes 5% contour). Acquired in the plane passing by the centre of effusion holes (for  $VR = 0.37$ ). (Bottom) side view of the experimental set-up.

In fact, exact correspondence between the temperature and momentum fields should never be expected. A clue to these differences lies in the fact that equations for both the mean temperature and mean-square temperature fluctuations do not contain terms for the pressure gradient while those for the momentum and turbulence kinetic energy do. Using direct numerical simulations, Guezennec et al. (1990) show that heat is a poor marker of the instantaneous vorticity field. They also show that, except very close to the wall, pressure-gradient forces are significantly larger than viscous forces (Batchelor & Townsend, 1956) but play no role in the exchange of heat. This is because velocity and pressure fluctuations extend over much shorter distances than temperature fluctuations, the latter stages of mixing of the scalar field occurring by molecular diffusion even though large eddies are brought together by mean flow advection and turbulent mixing. For a discussion of these challenges within the context of suddenly perturbed boundary layers, see Morrison (2005).

These ideas appear not yet to have been considered fully, owing partly to the difficulty of making the necessary measurements at high Reynolds numbers, which are a prerequisite for rational modelling techniques for film cooling design. This is the purpose of the current set of experiments.

## 2. Experimental setup

The large-scale, low-velocity experiment was carried out in the closed-loop 10x5 wind tunnel at Imperial College. The

## Instructions for the preparation of papers

incoming boundary layer was generated using a large, self-similar turbulent boundary layer, tripped and developed over 15 m, yielding a range of Reynolds numbers  $2700 < u_t \delta / \nu < 4700$ , with  $u_t$  the friction velocity and  $\delta \approx 0.2$  m the boundary layer thickness upstream of the plate (Figure 1). This turbulent boundary layer was perturbed with a geometrically similar effusion panel fed through a plenum supplied with compressed air and enclosed with a thick perforated plate. The temperature can be independently controlled, although in the present experiment, all measurements are isothermal. The effusion film was generated through a staggered grid of inclined  $D=16$  mm diameter holes with a pitch of  $5D$ . Time-resolved planar PIV data were acquired in a streamwise wall-normal plane above the effusion plate, along the hole centres, as shown in Figure 1. Visualisation images were acquired in the same way, but with targeted seeding. This allows us to reconstruct the concentration  $C$  of injected fluid (saturated with seeding) with respect to incoming flow (largely unseeded) using the scattered light intensity as a surrogate for concentration.

$$C_{\%}(x, y, t) = \frac{I(x, y, t) - I_{min}}{I_{max} - I_{min}} \times 100 \quad (1)$$

Here,  $I(x, y, t)$  is the light intensity at position  $(x, y)$  of the visualization image acquired at time  $t$ , and  $I_{min}$  and  $I_{max}$  are the minimal light intensity (far field) and maximal light intensity (directly out of the effusion holes), respectively. Since enough residual particles are still present everywhere in the flow, velocity fields can be calculated synchronously with concentration fields. A wide range of low velocity ratios were investigated, in the range  $0 < VR < 0.4$  with the holes open. For  $VR=0$ , hole discontinuity is the only change of boundary conditions to the turbulent boundary layer. These data sets were complemented by hot-wire measurements of the streamwise velocity.

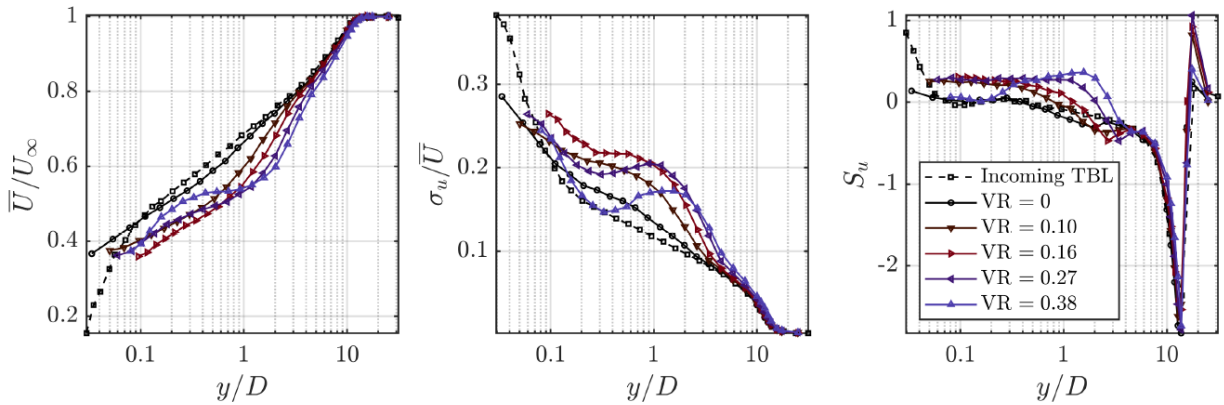


Figure 2: Streamwise velocity statistics from hot-wire measurements. Plain lines correspond to profiles at  $(x = 594 \text{ mm} = 37.1D, z = 40 \text{ mm} = 2.5D)$  mid-way between two rows of effusion holes. Colours from dark to light depict different effusion cases  $VR = \{0, 0.10, 0.16, 0.27, 0.38\}$ , respectively.

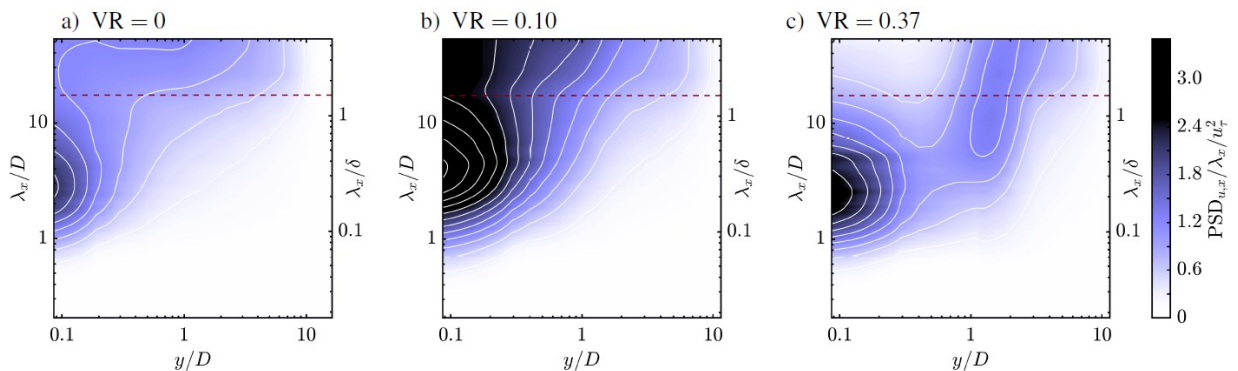


Figure 3: Pre-multiplied power spectral densities of streamwise velocity  $PSD_{u,x}$  as a function of wavelength  $\lambda_x$  and wall distance  $y$  for three  $VR$ , from PIV datasets along centre-line of holes. Contour levels are shown every  $0.3 u_t^2$ . The horizontal dashed lines mark the cut-off wavelength  $\lambda_x = 1.5\delta$ .

### 3. Discussing results

Measurements of the streamwise velocity component are performed with a single hot wire. Figure 2 shows wall-normal profiles of the first- ( $\bar{U}/U_\infty$ ), second- ( $\sigma_u/\bar{U}$ ) and third-order moments (skewness,  $S_u$ ) acquired mid-way between two adjacent rows of holes. The mean velocity profile of the perturbed boundary layers no longer shows the log-law

exhibited by the incoming boundary layer. The roughness of the effusion holes also results in lower turbulence rate in the near-wall region due to enhanced mixing. When  $VR > 0$ , the turbulence rate first increases throughout the boundary layer. With increasing  $VR$  the levels of turbulence concentrate around  $D < y < 3D$ , corresponding to film lift-off.

Typically, the skewness upstream of the effusion panel is significant ( $0 < S_u < 1$ ) close to the wall, is zero in the buffer layer and log layer and then decreases to large negative peak ( $S_u \approx -3$ ) at edge of the boundary layer due to the highly contorted turbulent / non-turbulent interface. Like the turbulence rate, the roughness layer induced by the perforated plate drastically attenuates the skewness close to the wall but leaves the rest of the BL unchanged. The introduction of the effusion film increases the skewness significantly in the buffer layer. This evolution suggests a higher correspondence between high momentum events and the enhancement of the turbulent kinetic energy.

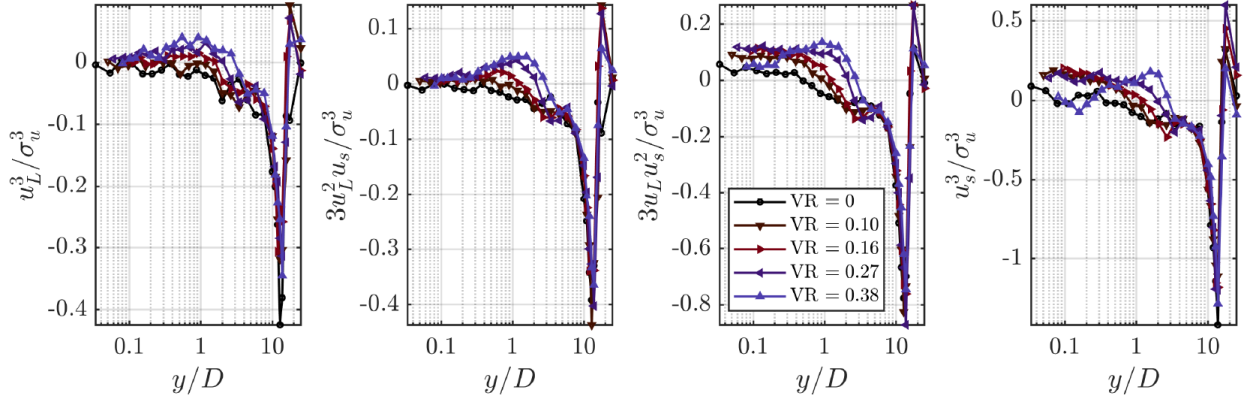


Figure 4: Skewness decomposition into large and small scales, from hot-wire measurements. Profiles are obtained at ( $x = 594 \text{ mm} = 37.1D$ ,  $z = 40 \text{ mm} = 2.5D$ ) mid-way between two rows of effusion holes. Colours from dark to light depict different effusion cases  $VR = \{0, 0.10, 0.16, 0.27, 0.38\}$ , respectively.

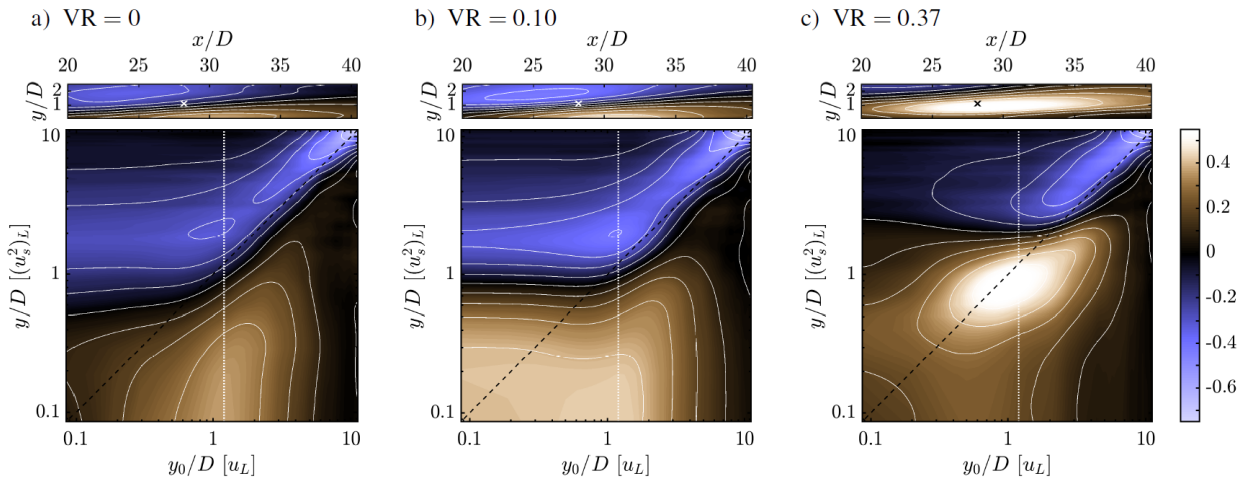


Figure 5: Amplitude modulation coefficient for (a)  $VR = 0$ , (b)  $VR = 0.10$ , and (c)  $VR = 0.37$ . (Top) single point correlation  $AM(x, y)$  at reference point ( $x_0 = 28D$ ,  $y_0 = 1.2D$ ), and (bottom) two-point correlation profile  $AM(y_0, y)$  at  $x_0 = 28D$ . White vertical dotted lines mark the intersections with top maps at  $y_0 = 1.2D$  and black dashed diagonals mark the no-shift correlation ( $y = y_0$ ).

Further insight from the skewness is provided by separating fluctuations into two distinct ranges: large-scale motions and small-scale turbulence. To that aim, the spectral signature of the streamwise velocity in the perturbed boundary layer is depicted in Figure 3, where pre-multiplied spectrograms are calculated using PIV velocity fields. For  $VR=0$ , the behaviour is consistent with high Reynolds number boundary layers (Ganapathisubramani et al., 2005; Squire et al., 2016; Basley et al., 2018). There is a scale separation between small-scale turbulence confined in the roughness sublayer – here generated by the perforated plate – and large-scale motions that are particularly intense in the log layer. The gap between small scale turbulence populating the ‘roughness sublayer’ and the large-scale motions allows for the decomposition of velocity fluctuations into  $u = u_L + u_s$ , where  $u_L = u(\lambda_x > 1.5\delta)$  is the large-scale component

## Instructions for the preparation of papers

obtained through unbiased lowpass filtering, while  $u_s$  represents the remaining fluctuations at smaller scales. With this decomposition, the skewness can be defined as in Equation (2),

$$Su = \frac{\langle u^3 \rangle}{\sigma_u^3} = \frac{\langle u_L^3 \rangle + 3\langle u_L^2 u_s \rangle + 3\langle u_L u_s^2 \rangle + \langle u_s^3 \rangle}{\sigma_u^3} \quad (2)$$

where  $\langle \cdot \rangle$  denotes time averaging. The decomposition of the skewness profile seen in Figure 2 is plotted in Figure 4. Except for the negative spike close to  $y = \delta$  (typical of the turbulent / non-turbulent interface), these expansion terms show the relative effects of large- and small-scale processes in inter-scale exchanges.

Triadic exchanges within the large-scale range exclusively are associated with  $\langle u_L^3 \rangle$ . They remain near zero. The term  $\langle u_L^2 u_s \rangle$  represents the influence of small scales on the amplitude of large-scale fluctuations. It is weak but, interestingly, goes from negative at low VR to positive when VR increases significantly. This might be indicative of the appearance of intermediate scales generated by the introduction of the film. The terms  $\langle u_s^3 \rangle$  and  $\langle u_L u_s^2 \rangle$  relate to the amplitude of small-scale turbulence. The former represents exclusively small-scale, triadic exchanges (skewness), while the latter corresponds to correlations between large-scale fluctuations and the amplitude of small-scale fluctuations. Both terms become increasingly positive for low  $VR < 0.3$ . However, at the highest velocity ratio,  $VR = 0.37$ , this trend reverses and values tend to zero near the wall. On the contrary, the correlation between small-scale turbulence and large-scale motions keeps increasing at the top of the film ( $D < y < 2D$ ) with increasing VR. This indicates that the injection of the film indeed promotes mixing with the incoming boundary layer, but the increasing VR changes the nature of the film under the mixing layer which is pushed further away from the wall.

Mathis et al. (2011) have highlighted the relationship between the skewness expansion in Equation (2), specifically the term  $\langle u_L u_s^2 \rangle$ , and the amplitude modulation approach used in numerous papers recently (Mathis et al., 2009; Marusic et al., 2010; Mathis et al., 2011). This approach consists in quantifying the amplitude modulation of small-scale turbulence by large-scale motions as a correlation coefficient between large scales  $u_L$  and  $(u_s^2)_L$ , the large-scale envelope of small-scale fluctuations, obtained by low-pass filtering  $u_s^2$ .

Often restricted to temporal correlations of hot-wire measurements, AM has recently been extended to two-point spatial correlations (Basley et al., 2018; Yao et al., 2018). Inclined, meandering large-scale motions modulate the amplitude of small scales in the roughness sublayer, so that turbulence is intensified directly beneath these large structures. Here, the single-point modulation coefficient is calculated with respect to the large-scale motions at a reference position denoted  $(x_0, y_0)$ :

$$AM(x_0, y_0, x, y) = \frac{\langle u_L(x_0, y_0) * (u_s^2)_L(x, y) \rangle}{\sigma_{u_L}(x_0, y_0) \sigma_{(u_s^2)_L}(x, y)} \quad (3)$$

where  $s$  denotes a standard deviation. AM represents a generalization of the covariance between  $u_L$  and  $u_s^2$  that is the term  $\langle u_L u_s^2 \rangle$ . Figure 5 shows the momentum exchange between scales. At low VR the amplitude modulation is enhanced near the wall. As VR increases, the injection of momentum alters this mechanism, but amplitude modulation of small-scale turbulence still occurs. Notably, amplitude modulation is significantly amplified further from the wall at  $y \approx y_0 \approx D$ , corresponding to the mixing layer that hovers after the effusion film lifts off (see also Basley et al., 2021). The present work builds on these findings to expand the modulation approach to passive tracers within the effusion film.

The coefficient

$$\gamma_{u,c}(x_0, y_0, x, y) = \frac{\langle u_L(x_0, y_0) * c_L(x, y) \rangle}{\sigma_{u_L}(x_0, y_0) \sigma_{c_L}(x, y)} \quad (4)$$

quantifies the spatial correlation between the large-scale fluctuations of streamwise velocity at  $(x_0, y_0)$  and the large-scale fluctuations of concentration at  $(x, y)$ . Examples of correlation maps are displayed in Figure 6. The reference point ( $x_0 = 28D; y_0 = 1.2D$ ) for the single-point maps (Figure 6 top) was chosen to depict a representative picture of the dynamics. Streamwise,  $x_0 = 28D$  is a midway point between two successive holes (5th and 6th), downstream enough for the sublayer to be established, while  $y_0 = 1.2D$  corresponds to the edge of the sublayer where the high levels of kinetic energy were measured. The two-point correlation maps (Figure 6 bottom) identify correlations between distant features of the flow, taken at different wall-distance.

Two regimes can immediately be identified from these maps. For low velocity ratio  $VR = 0.10$ , there is a strong local anti-correlation between concentration and momentum within the film confined near the wall. The distribution in Figure 6(a) top is inclined as it follows the flow in the sublayer. This signature results from the injected fluid carrying relatively less momentum compared to the incoming flow. The modulation by outer-layer dynamics is non-existent.

The scenario for higher velocity ratio  $VR = 0.37$  is completely different (Figure 6b). Since the local anti-correlation with local velocity fluctuations is the signature of recently injected (unmixed) fluid, it is logically pushed much further away from the plate. However, a stronger modulation appears in the near-wall region of the effusion film with the distant large-scale motions in the outer-layer, as shown by the bottom right corner of Figure 6(b) bottom.

This implies that, despite keeping the large-scale motions away from the near-wall region, higher VR cases enhance rather than reduce the influence of incoming turbulence on the injection of the effusion film. Such a remote correlation between large-scale motions and near-wall concentration of injected fluid suggests an interplay via wall pressure and is the subject of ongoing work.

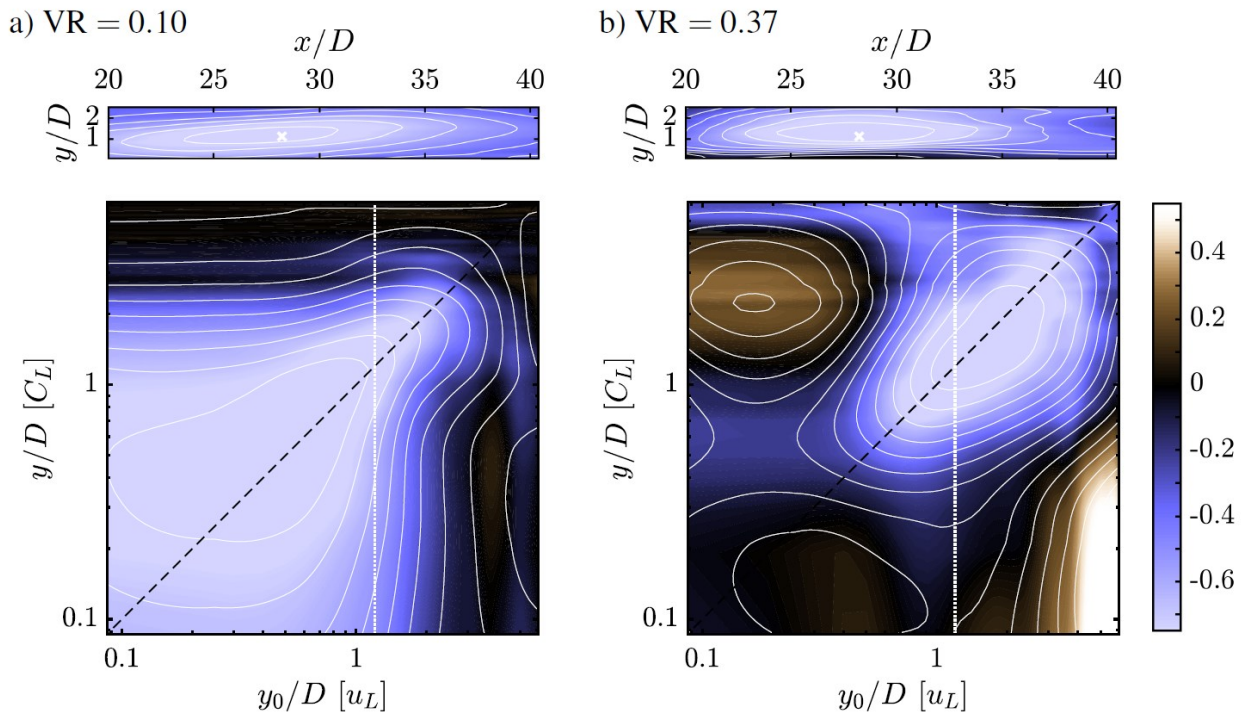


Figure 6: Correlation coefficient maps between large-scale fluctuations of velocity and large-scale fluctuations of concentration for two VR cases. (Top) single point correlation  $\gamma_{u,c}(x,y)$  at reference point  $(x_0 = 28D, y_0 = 1.2D)$ , and (bottom) two-point correlation  $\gamma_{u,c}(y_0, y)$  at  $x_0 = 28D$ . White dotted lines mark the intersections with top maps at  $y_0 = 1.2D$  and black dashed diagonals mark the no-shift correlation ( $y = y_0$ ).

#### 4. Concluding remarks

This study comes within the framework of turbine blade effusion cooling. This paper highlights the importance of film detachment at much lower VRs than typically used in gas turbines. The underlying mechanisms of the mixing and breaking-up of an effusion film are investigated in an idealized case of a canonical turbulent boundary layer.

The mixing of passive tracers injected with the effusion film is analysed in depth with respect to synchronous PIV data. This results in joint data sets of concentration and momentum fields, which reveal a striking change in the dynamics of the perturbed boundary layer when velocity ratios exceed  $VR = 0.15$ : from low-momentum diffusion confined to the near-wall region, where mixing is limited to small-scale turbulence, the injected sublayer breaks up to shreds drifting towards the edge of the outer layer, where more intense mixing occurs. Consequently, not only the excessive momentum of higher VR promotes mixing of the film, but it also renders the near-wall film more susceptible to intense modulations by large-scale motions passing in the outer layer.

## Instructions for the preparation of papers

It is worthwhile noting the threshold  $VR=0.15$  is likely quite sensible to geometry and flow conditions. However, this value is remarkably low with respect to typical velocity ratios encountered in gas turbines, generally well over  $VR=1$ . The resulting time-resolved and space-extended data sets explain the favourable outcome of low velocity ratios, for which the shear-driven mixing of the effusion film is limited to near-wall region of the boundary layer. Results also suggest that the effusion film effectively restricts the penetration of fluid from the outer region into the near-wall region of the boundary layer.

### References

- [1] Andreopoulos, J. 1983 The response of a turbulent boundary layer to a double step-change in a wall heat flux. *ASME J. Heat Transfer* 105, 841–845.
- [2] Basley, J., Gouder, K. & Morrison, J. F. 2021 Large-scale modulation of an effusion film by a turbulent boundary layer. In *Proceedings of ICTAM 2020+1*, online.
- [3] Basley, J., Perret, L. & Mathis, R. 2018 Spatial modulations of kinetic energy in the roughness sublayer. *J. Fluid Mech.* 850, 584–610.
- [4] Batchelor, G. K. & Townsend, A. A. 1956 Turbulent diffusion. In *Surveys in Mechanics* (ed. G. K. Batchelor & R. M. Davies). Cambridge University Press.
- [5] Ganapathisubramani, B., Hutchins, N., Hambleton, W. T., Longmire, E. K. & Marusic, I. 2005 Investigation of largescale coherence in a turbulent boundary layer using two-point correlations. *J. Fluid Mech.* 524, 57–80.
- [6] Guezennec, Y., Stretch, D. & Kim, J. 1990 The structure of turbulent channel flow with passive scalar transport. In *Studying Turbulence Using Numerical Simulations Databases III*, 1990 Summer Program, p. 127. CTR Stanford / NASA Ames.
- [7] Kays, W. M. & Moffat, R. J. 1988 The near wall region of the turbulent boundary layer: some results from heat transfer measurements. In *Zoran Zaric Memorial Conference on Near-Wall Turbulence* (ed. S. J. Kline & N. H. Afgan).
- [8] Krewinkel, R. 2013 A review of gas turbine effusion cooling studies. *Int. Journal of Heat and Mass Transfer* 66, 706–722.
- [9] Marusic, I., Mathis, R. & Hutchins, N. 2010 Predictive model for wall-bounded turbulent flow. *Science* 329 (193).
- [10] Mathis, R., Hutchins, N. & Marusic, I. 2009 Large-scale amplitude modulation of the small-scale structures in turbulent boundary layers. *J. Fluid Mech.* 628, 311–337.
- [11] Mathis, R., Marusic, I., Hutchins, N. & Sreenivasan, K. R. 2011 The relationship between the velocity skewness and the amplitude modulation of the small scale by the large scale in turbulent boundary layers. *Physics of Fluids* 23 (12), 121702.
- [12] Morrison, J. F. 2005 Boundary layers under strong distortion: an experimentalist's view. In *Prediction of turbulent flows* (ed. G. F. Hewitt & J. C. Vassilicos), pp. 163–206. Cambridge University Press.
- [13] Smits, A. J. & Wood, D. H. 1985 The response of turbulent boundary layers to sudden perturbations. *Ann. Rev. Fluid Mech.* 17, 321–358.
- [14] Squire, D. T., Morrill-Winter, C., Hutchins, N., Schultz, M. P., C., Klewicki J. & Marusic, I. 2016 Comparison of turbulent boundary layers over smooth and rough surfaces up to high Reynolds numbers. *J. Fluid Mech.* 795, 210–240.
- [15] Subramanian, C. S. & Antonia, R. A. 1981 Response of a turbulent boundary layer to a sudden decrease in wall heat flux. *Int. J. Heat Mass Transfer* 24, 1641–1647.
- [16] Yao, Y. C., Huang, W. X. & Xu, C. X. 2018 Amplitude modulation and extreme events in turbulent channel flow. *Acta Mechanica Sinica* 34 (1), 1–9.